Monthly Notices
of the
ROYAL ASTRONOMICAL SOCIETY

Mon. Not. R. Astron. Soc. **405,** 2471–2484 (2010) doi:10.1111/j.1365-2966.2010.16624.x

New 9.9-GHz methanol masers

M. A. Voronkov,[1,2⋆] J. L. Caswell,[1] S. P. Ellingsen[3] and A. M. Sobolev[4]

[1]*Australia Telescope National Facility, CSIRO Astronomy and Space Science, PO Box 76, Epping, NSW 1710, Australia*
[2]*Astro Space Centre, Profsouznaya st. 84/32, 117997 Moscow, Russia*
[3]*School of Mathematics and Physics, University of Tasmania, GPO Box 252-37, Hobart, Tasmania 7000, Australia*
[4]*Ural State University, Lenin ave. 51, 620083 Ekaterinburg, Russia*

Accepted 2010 March 2. Received 2010 March 2; in original form 2009 December 10

ABSTRACT

The Australia Telescope Compact Array has been used to make the first extensive search for the class I methanol masers at 9.9 GHz. In total, 48 regions of high-mass star formation were observed. In addition to masers in W33-Met (G12.80−0.19) and G343.12−0.06 (IRAS 16547−4247) which have already been reported in the literature, two new 9.9-GHz masers have been found towards G331.13−0.24 and G19.61−0.23. We have determined absolute positions (accurate to roughly a second of arc) for all the detected masers and suggest that some class I masers may be associated with shocks driven into molecular clouds by expanding H II regions. Our observations also imply that the evolutionary stage of a high-mass star-forming region when the class I masers are present can outlast the stage when the class II masers at 6.7-GHz are detectable, and overlaps significantly with the stage when OH masers are active.

Key words: masers – stars: formation – ISM: H II regions – ISM: molecules.

1 INTRODUCTION

Methanol masers are well-established probes of high-mass star formation. They are divided into two categories first defined by Batrla et al. (1987): class II masers (of which the 6.7 GHz is the best known and usually the strongest) are associated with millimetre and infrared sources (e.g. Hill et al. 2005) and reside in the close environment of high-mass young stellar objects (YSOs). Class I masers (of which the 44 and 95 GHz are commonly observed) are often found apart from the strong continuum and infrared sources and can be separated by up to a parsec from the YSO responsible for excitation (e.g. Kurtz, Hofner & Álvarez 2004; Voronkov et al. 2006; Cyganowski et al. 2009).

Theoretical calculations are able to explain this empirical classification and strongly suggest that the pumping process of class I masers is dominated by collisions with the molecular hydrogen (see e.g. Lees 1973; Sobolev & Strelnitskii 1983; Voronkov 1999) in contrast to class II masers, which are pumped by radiative excitation (see e.g. Wilson et al. 1985; Sobolev & Deguchi 1994; Sutton et al. 2001). The two pumping mechanisms were shown to be competitive (see e.g. Menten 1991; Cragg et al. 1992; Voronkov 1999; Voronkov et al. 2005b). For example, strong radiation from a nearby infrared source quenches class I masers and increases the strength of class II masers (Voronkov et al. 2005b). Although it has been demonstrated by theoretical calculations that a weak class II maser at 6.7 GHz can coexist with a bright class I emission under special conditions (Voronkov et al. 2005b), bright masers of different classes residing in the same volume of gas are widely accepted as mutually exclusive. However, on larger scales, they are often observed to coexist in the same star-forming region within less than a parsec of each other.

Class I methanol masers are relatively poorly studied. The common consensus is that the majority of class I masers trace interface regions between outflows and molecular gas, although direct observational evidence of this has been obtained for a limited number of sources only (e.g. Plambeck & Menten 1990; Kurtz et al. 2004; Voronkov et al. 2006). An alternative scenario, which involves cloud–cloud collisions, may be realized in some sources (Sobolev 1992; Mehringer & Menten 1996; Salii, Sobolev & Kalinina 2002). The common ingredient of these two scenarios is the presence of shocks. There is observational evidence that the methanol abundance is significantly increased in the shock-processed regions (e.g. Gibb & Davis 1998; Sutton et al. 2004). The gas in such regions is heated and compressed increasing the frequency of collisions with molecular hydrogen and, therefore, providing a more efficient pumping (e.g. Sutton et al. 2004). Chen, Ellingsen & Shen (2009) demonstrated statistically the association of class I masers with the shocks traced by extended features showing a prominent excess of the 4.5-μm emission in the images obtained with the *Spitzer Space Telescope*'s Infrared Array Camera (IRAC) also known as extended green objects (EGOs; Cyganowski et al. 2008).

To date, there is observational evidence that more than 20 methanol transitions can produce class I masers, more than half of which belong to the J_2–J_1 E series in the 25–30 GHz frequency range (Voronkov 1999; Müller, Menten & Mäder 2004). The

⋆E-mail: maxim.voronkov@csiro.au

observational properties of different class I masers are not the same. Some masers, e.g. at 44 and 95 GHz, are known to be quite ubiquitous with about 100 sources known to date (see e.g. Haschick, Menten & Baan 1990; Slysh et al. 1994; Val'tts et al. 2000; Kurtz et al. 2004; Cyganowski et al. 2009). On the other hand, there are other transitions with very few known maser sources. An example of such a transition showing rare maser activity is the 9_{-1} to 8_{-2} E methanol transition at 9.9 GHz. The rarity of these masers is likely due to the strong dependence of the maser brightness on the physical conditions, especially in the requirement of higher typical temperatures and densities for these masers to form (Sobolev et al. 2005).

Slysh, Kalenskii & Val'tts (1993) conducted the only search for the 9.9-GHz masers reported in the literature so far. However, they observed just 11 targets which were largely well-known regions of high-mass star formation where methanol masers of either class had previously been reported and discovered a single 9.9-GHz maser (W33-Met, also known as G12.80−0.19). In this paper we report the results of the search for the 9.9-GHz masers towards 48 independent positions. The majority of targets, 46 sources in total, were known class I masers at 44 and/or 95 GHz drawn from Slysh et al. (1994), Val'tts et al. (2000), Kurtz et al. (2004) and Ellingsen (2005). The remaining two sources were included in order to cover all known star-forming regions located south of declination of -20°, which have a periodically variable class II methanol maser at 6.7-GHz according to Goedhart, Gaylard & van der Walt (2004). Little is known about the physics of periodic variability of such masers. Therefore, a detection of the 9.9-GHz maser (which is very sensitive to the physical conditions and has a different pumping to the 6.7-GHz maser) in the same source might shed light on this enigmatic phenomenon.

2 OBSERVATIONS

Observations were made with the Australia Telescope Compact Array (ATCA) in seven time allocations scheduled from 2005 December to 2008 July (the archive project code is C1466). The details of these observing sessions along with the array configurations used and the range of baseline lengths are summarized in the first five columns of Table 1. Each source was observed in several (typically six) cuts of 10 min each to get a good hour angle coverage. The data reduction was performed using the MIRIAD package (2007 December 13 release) following standard procedures (with the exception of bandpass calibration). The bandpass calibration was achieved by fitting a low-order polynomial to the spectra of the bandpass calibrator (1921-293, except for the observations on December 17 and June 2, when 0537-441 and 1253-055 were observed, respectively) using the uvlin and mfcal tasks. This approach for bandpass calibration is usually superior and adds less noise than an independent solution for each spectral channel, if one tries to detect a weak narrow line in the presence of a strong continuum, which is the case for many sources in our sample.

The regular observations were preceded by a short test project (the archive project code is CX075) using Director's time in 2004 December and 2005 January. It aimed at testing the viability of observations at 9.9 GHz, which is outside the nominal range of the ATCA *X*-band receivers (8.0–9.2 GHz), but yielded the serendipitous discovery of a new 9.9-GHz maser in G343.12−0.06 (IRAS 16547−4247). This source was then investigated in detail in a separate paper (Voronkov et al. 2006). The receiver performance was found to vary significantly from antenna to antenna at 9.9 GHz due to the proximity of the band edge. In particular, baselines including antenna CA01 had approximately three times higher noise than other baselines in most sessions. As the masers are unresolved sources for the ATCA, this inhomogeneity in the sensitivity of individual baselines is taken care of automatically by the imaging process.

We adopted an astronomical measurement of the rest frequency for the 9_{-1} to 8_{-2} E methanol transition, 9936.201 ± 0.001 MHz (Voronkov et al. 2006). The uncertainty corresponds to 0.03 km s^{-1} of the radial velocity. The adopted rest frequency lies within the uncertainty of the laboratory measurement of Müller et al. (2004) equivalent to 0.12 km s^{-1}. The correlator was configured with 1024 spectral channels across a 4-MHz bandwidth, providing a spectral resolution of 0.12 km s^{-1}. In addition, the spare correlator capacity was used to observe the 8.6-GHz continuum emission (with the 128-MHz bandwidth) simultaneously with the line measurement. Although two orthogonal linear polarizations have been recorded, the correlator configuration used in the project did not allow us to calibrate the instrumental polarization and hence to determine

Table 1. Dates of observations, a summary of array configurations and decorrelation estimates. More details on the ATCA configurations are available on the web (http://www.narrabri.atnf.csiro.au/observing/configs.html). Note that antenna CA01 did not perform well at this frequency in 2005/2006. It is involved, in particular, in the shortest spacing of the 6C array configuration. Therefore, the shortest baseline was not as sensitive as the other baselines in the March observations. Antenna CA06 did not observe in the 2008 sessions.

UT date of observations	Array configuration	Baseline length Min (m)	Max no CA06 (m)	Max with CA06 (m)	Decorrelation estimate Source and calibrator	Separation Angular (°)	Temporal (min)	Estimated factor
2005 December 15	6A	337	2923	5939	1059-63 (odd + even)	0	23.8 (2)	3.8 (7)
					1613-586 (odd + even)	0	21 (5)	5.7 (5)
2005 December 16					1613-586 (odd + even)	0	18 (3)	6.8 (4)
2005 December 17					1613-586 (odd + even)	0	17 (3)	1.88 (3)
2006 March 25	6C	153	2786	6000	1646-50 (odd + even)	0	27.8 (1)	1.179 (4)
					1710-269 + 1730-130	14.6	20.1 (7)	1.25 (1)
2006 March 26					1646-50 (odd + even)	0	20.4 (2)	1.14 (2)
					1710-269 (odd + even)	0	21 (1)	1.250 (9)
2008 June 2	EW352	31	352	none	1646-50 (odd + even)	0	17 (2)	1.004 (5)
2008 July 20	H214	92	247	none	1646-50 (odd + even)	0	9 (2)	1.036 (2)
					1613-586 (odd + even)	0	9 (2)	1.065 (3)
					1646-50 + 1613-586	9.3	1.8 (1)	1.16 (2)

polarization properties of the observed emission. During the data reduction, the orthogonal polarizations were converted to Stokes-I. Therefore, all flux densities presented in the paper are not affected by polarization to the first order.

All image cubes were constructed from the visibility data after continuum subtraction. The natural weights were used providing a typical synthesized beam size of around a few seconds of arc. Due to software limitations the search area was split into nine subcubes with a 50 per cent overlap. Each subcube containing 512 × 512 spatial pixels of 0.5 × 0.5 arcsec^2 and 1024 spectral channels was then processed separately. This strategy covered a rectangular area of 8.3 arcmin in size. The half-power width of the primary beam is 5.1 arcmin at this frequency. An automated spectral line finder (Voronkov, in preparation) based on the ATNF Spectral line Analysis Package (http://www.atnf.csiro.au/computing/software/asap) was used to search for sources in the dirty spectral cubes.[1] The spectral line finder applied a simple statistical criterion of at least three consecutive spectral channels above the threshold of 3σ (with respect to the noise in the local vicinity of the tested channels) to claim a detection. The three-dimensional search routine formed slices along the spectral axis for each spatial pixel, ran the one-dimensional algorithm and combined the results into sources. The sources which had less than four spatial pixels with detected emission (half-power area of the main lobe of synthesized beam) were discarded. Due to statistical noise fluctuations, the algorithm produced of the order of 10 spurious sources per cube, each of which was examined manually. The same source detection software was used and thoroughly tested in the Parkes 6-GHz Multibeam survey (hereafter MMB survey; Green et al. 2009). In addition to automated software, both single baseline and averaged uv spectra (visibility amplitude versus frequency) were inspected by eye to search for possible broad thermal components, which may not be imaged adequately with the uv coverage provided by the sparse ATCA configurations. Due to the low dynamic range in the dirty image cubes the automated software reported a number of detections around the field of view for each real maser. In this case, a deconvolved cube was made using the CLEAN task and the source parameters were measured using the imfit task of MIRIAD. A self-calibration was performed and a new cube was constructed after the absolute position had been determined. The spectra were extracted from such self-calibrated cubes using the imspec task. An additional search for weaker masers was performed in the parts of the self-calibrated cube unaffected by the main maser feature using the same approach as for the original cubes. However, we did not find any additional weak maser features.

During the first two observing allocations of the regular observations in 2005 December the atmospheric conditions were very unstable with thunderstorms present in the area causing an interruption once on December 15. Observations through adverse weather, aggravated by the sparse array configuration, resulted in an increased level of decorrelation due to a poor phase stability. As this decorrelation directly affects the flux density limit for all non-detections, we have attempted to estimate it using the calibrator data. We used two different methods, depending on the data available for a particular observing session. On March 25 two separate continuum calibrators 1710-269 and 1730-130 were observed using the same frequency setup, which was chosen to achieve an appropriate velocity range for the target sources. The first source of this pair acted as an ordinary secondary calibrator allowing us to form a calibration solution. The second source was then imaged using this calibration. Another image of the second source was constructed following a self-calibration. Then, the decorrelation factor was measured as the ratio of the two flux densities obtained from each image using the imfit task. The second method, suitable for observations with only one calibrator, is to split the whole sequence of calibrator scans into odd and even scans and then treat the odd ones as a calibrator and the even scans as a source. The decorrelation factor was then obtained from the images the same manner as for the first method.

The right-hand four columns of Table 1 summarize the results for each observing session, including the method and sources used, angular and mean temporal separation between them would be target and calibrator, and the estimated decorrelation factor. The uncertainties are expressed in the units of the least significant figure. Table 1 shows that the decorrelation was up to seven times worse during the first two observing sessions. It is worth noting that these estimates are likely to be larger than the actual decorrelation affecting the target sources because we effectively double the length of the calibrator cycle when splitting calibrator scans into odd and even scans. For some observing sessions more than one decorrelation estimate is available (Table 1). The estimates are in a good agreement for the session on December 15, when the phase stability was bad, but are more than 3σ apart for the March sessions, which had a good phase stability. This is likely to be due to systematic effects such as different declinations for the calibrators involved in the estimates (which makes the average elevations different), and an additional angular separation when a pair of sources was used instead of the odd + even method. We used the largest decorrelation estimate obtained for each observing session to scale the flux density limits for non-detections.

The last two sessions in 2008 (Table 1) were completely devoted to the 9.9-GHz maser discovered towards G331.13−0.24 during the session on December 16 and no new targets were observed. The goal of these repeated observations was to provide an independent measurement of the absolute position of the maser. We found that the morphology of G331.13−0.24 was such that an independent estimate of a systematic uncertainty was required for an unambiguous interpretation. A typical (1σ) astrometric accuracy of ATCA (largely determined by systematic effects for masers) is usually adopted to be around 0.5 arcsec. However, the bad weather of the December 16 session is likely to have further degraded the accuracy. Although two 2008 sessions used relatively compact array configurations and the synthesized beam was an order of magnitude larger, by observing in good weather and by using a different calibrator (1646-50 instead of 1613-586) for which a more accurate position is available, we have achieved a comparable formal uncertainty of the position measurement in all three sessions. We found that the absolute positions obtained in all three sessions are consistent, and we estimate the final accuracy (sigma for the mean) to be 1 arcsec.

3 RESULTS

In addition to the new 9.9-GHz maser found in G343.12−0.06 during the pilot survey as a chance discovery (results of the follow-up are reported in Voronkov et al. 2006), the regular survey yielded three other detections, listed in Table 2. These include the known 9.9-GHz maser in W33-Met (G12.80−0.19) discovered by Slysh et al. (1993), and two new detections. The first six columns of the table are self-explanatory and include the date of observation, the synthesized beam size and its position angle (PA), the noise level

[1] Strictly speaking, sidelobes are only caused by real sources. Therefore, no deconvolution is required unless there is a detection.

Table 2. Observation details for sources detected at 9.9 GHz. All uncertainties are given in the brackets and expressed in the units of the least significant figure. The uncertainty of the decorrelation factor was calculated from the uncertainties of the flux measurement.

Source name	Date of observation	Synthesized beam FWHM (arcsec)	Synthesized beam PA (°)	1σ noise level (mJy beam^{-1})	Inspected velocity range (km s^{-1})	Measured decorrelation factor	Separation from calibrator Angular (°)	Separation from calibrator Temporal (min)
G331.13−0.24	2005 December 16	2.1 × 1.5	15	39	−124, −27	2.9 (3)	7.0	5.3 (1)
	2008 June 2	18 × 12	3	35	−131, −34	1.04 (2)	6.2	4.0 (1)
	2008 July 20	17 × 14	53	68	−150, −53	1.09 (3)	6.2	4 (1)
W33-Met	2006 March 25	2.6 × 1.0	14	44	−29, +53	1.18 (4)	11.0	5.4 (1)
G19.61−0.23	2006 March 25	3.7 × 1.0	7	43	−28, +68	1.60 (6)	13.4	21 (3)

in the image representing the detection threshold and the velocity range searched for maser emission. The last three columns are related to the decorrelation estimates. For sources with a maser detection, self-calibration effectively provides a measurement of the decorrelation factor. The factor given in Table 2 was calculated as the ratio of the flux density obtained using a self-calibrated data set of the maser to that prior to the self-calibration. The values are below the estimates obtained for a particular observing session using the calibrator data (see Table 1) as they are expected to be, with the exception of the last source, G19.61−0.23. For this source, the measured decorrelation is slightly higher than the estimate deduced from the calibrator data. This fact can probably be explained by a more northern location of the source than either of the calibrators used for decorrelation estimates and, as a result, a lower elevation on average throughout the observing run. Systematic effects such as fit errors due to the elongated synthesized beam along the declination axis, which is produced by the east–west arrays for the sources located near the equator, could also contribute to this minor discrepancy. For the purpose of comparison, the last two columns of Table 2 give the angular and temporal separation of the maser source from the appropriate secondary calibrator. The uncertainties are given in round brackets and expressed in the units of the least significant figure.

The absolute position, peak velocity and flux density are summarized in Table 3 for all detected masers. We have added G343.12−0.06 (Voronkov et al. 2006) so that Table 3 contains a complete list of all four 9.9-GHz masers known to date. The uncertainty of the peak velocity is the spectral resolution given in the previous section (the rest frequency uncertainty is much smaller than the spectral resolution). The flux density uncertainties given in Table 3 are cumulative values including both the image noise given in Table 2 and the accuracy of the flux scale calibration, which is typically of the order of 3 per cent at centimetre (cm) wavelengths. The spectra of the 9.9-GHz detections are shown in Fig. 1. All masers have simple spectra in this transition containing just one component. In contrast, most sources have multiple components in the spectra of the most widespread class I methanol maser transition at 44 GHz (Slysh et al. 1994; Kogan & Slysh 1998). This situation is similar to that observed in G343.12−0.06, where the 9.9-GHz maser and other rare class I masers at 25 and 104 GHz are confined to one spot only, while the more widespread 95- and 84-GHz masers have been observed in a number of spots (Voronkov et al. 2006). Such a behaviour confirms the hypothesis that the 9.9-GHz masers are produced under a more restricted range of physical conditions than the widespread masers.

Fig. 2 shows positions of detected 9.9-GHz masers with respect to the 8.6-GHz continuum observed simultaneously. The positions of the 6.7-GHz masers (see notes on individual sources for references) are also shown. The grey-scale represents the *Spitzer* IRAC 4.5-μm images. For one source, G331.13−0.24, we used the continuum data of Phillips et al. (1998). Both the morphology of the H II region and the flux density obtained in our measurement are in a good agreement with Phillips et al. (1998). But the map of Phillips et al. (1998), with better positional accuracy and uv coverage than in our measurement, reflects better the relative offset between the 6.7-GHz maser and the H II region.

The list of sources without a 9.9-GHz detection is given in Table 4. The first seven columns are self-explanatory and include the source name, the date of observations, observed position and velocity range searched for maser emission as well as the synthesized beam size [given as the full width at half-maximum (FWHM)] and its PA. The eighth column contains the noise level (1σ) in the

Table 3. The only four known masers at 9.9 GHz. In addition to three sources reported in this paper we have included G343.12−0.06 (Voronkov et al. 2006) for completeness. The uncertainties in the absolute positions given in the table are based on the formal uncertainty of the fit and the uncertainty of calibrator position. The commonly adopted systematic uncertainty (1σ) of the absolute positions measured with ATCA is 0.5 arcsec. All uncertainties in the table are given in the units of the least significant figure. The flux density uncertainty includes both the image noise (see Table 2) and the accuracy of the absolute flux scale calibration. The uncertainty of the peak velocity is the spectral resolution.

Source name	Date of observation	l (°)	b (°)	Determined position α_{2000} (h m s)	Determined position δ_{2000} (° ′ ″)	Peak velocity (km s^{-1})	Flux density (Jy)
G331.13−0.24	2005 December 16	331.131	−0.245	16:10:59.76 (5)	−51:50:26.9 (4)	−91.16	1.92 (7)
	2008 June 2			16:10:59.51 (3)	−51:50:26.1 (3)	−91.15	3.1 (1)
	2008 July 20			16:10:59.63 (3)	−51:50:27.3 (3)	−91.16	2.6 (1)
G343.12−0.06	2005 June 16	343.121	−0.064	16:58:16.460 (2)	−42:52:25.73 (3)	−31.56	9.5 (3)
W33-Met	2006 March 25	12.796	−0.192	18:14:10.897 (3)	−17:55:58.42 (8)	+32.72	4.3 (1)
G19.61−0.23	2006 March 25	19.608	−0.232	18:27:37.475 (2)	−11:56:37.77 (8)	+41.24	3.3 (1)

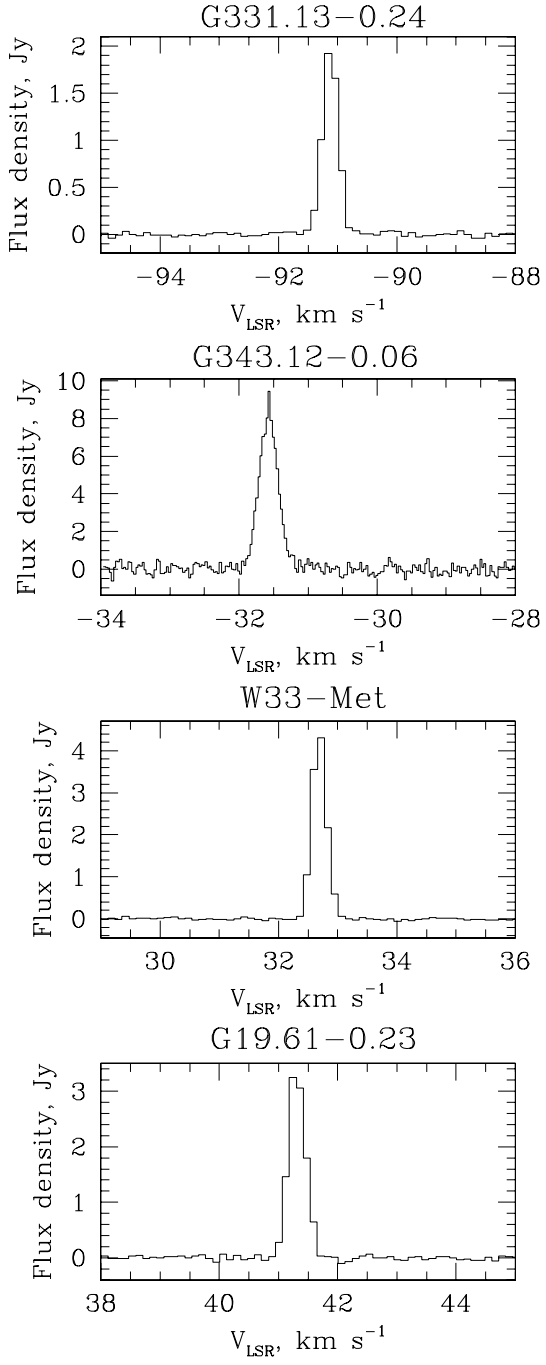

Figure 1. Spectra of the masers detected at 9.9 GHz. The uncertainty in radial velocity due to the rest frequency uncertainty is less than the spectral resolution. For completeness, we show the spectrum of G343.12−0.06 (from Voronkov et al. 2006). Note that the spectrum of this source was obtained with four times better spectral resolution, which is comparable with the rest frequency uncertainty.

dirty cubes searched for masers. This raw value does not take into account decorrelation due to weather, which we estimated using the calibrator data (Table 1). As mentioned above, we adopted the largest estimate of the decorrelation factor obtained for the particular observing slot. The cube noise level scaled with this factor is given in the ninth column of Table 4 as the estimate of the true 1σ detection limit. As this limit is likely to be overestimated a bit for the majority of sources observed in a bad weather we give the mean temporal and angular separation from the appropriate secondary calibrator in the last columns of Table 4. The smaller the separation, the lower the actual detection limit is expected to be. The uncertainties are given in the round brackets and expressed in the units of the least significant figure.

3.1 Notes on selected targets

In this section we discuss the sources where the 9.9-GHz masers were detected along with some non-detections. The latter are largely star-forming regions where an energetic interaction between outflow and molecular cloud has been reported in the literature, and therefore conditions favouring detection of the 9.9-GHz maser could be expected.

3.1.1 G301.14−0.23 (IRAS 12326−6245) non-detection

This source is deeply embedded in a dense molecular cloud and harbours one of the most energetic and massive bipolar molecular outflows known to date among objects of similar luminosity (Henning et al. 2000). There is a weak (∼1 Jy) class II methanol maser at 6.7 GHz with a peak velocity of −39.8 km s^{-1} (Caswell et al. 1995; Caswell 2009). It is associated with one of the two compact H II regions present in the source (Walsh et al. 1998). Within the uncertainty of the position measurement this maser is colocated with the mainline OH maser, which has features spread over unusually large velocity range from −64 to −35 km s^{-1} (Caswell & Haynes 1987; Caswell 1998). Voronkov et al. (unpublished observations) have detected a class I methanol maser at 25 GHz ($J = 5$ transition of the 25-GHz series) peaking at −36.0 km s^{-1} in this source. No 9.9-GHz maser emission has been detected in this source with the 1σ flux density limit of 0.4 Jy.

3.1.2 G305.21+0.21 possible detection

The class II methanol maser at 6.7 GHz in this source was observed at high angular resolution by Norris et al. (1993), who found two centres of activity separated by approximately 22 arcsec, labelled G305A and G305B following the notation of Walsh et al. (2007) or 305.208+0.206 and 305.202+0.208, respectively, according to Caswell (2009). There are two prominent H II regions in the source located approximately 30 arcsec to the south-east of G305A and 15 arcsec to the west of G305B, so none of the maser sites appear to be directly associated with any continuum emission (Phillips et al. 1998; Walsh et al. 2007). According to Walsh et al. (2007) the region G305A is a hot core active in a number of molecular tracers, while the state of G305B, which is associated with bright 8 μm emission is not fully clear.

This source was observed during the test 9.9-GHz survey without proper imaging. The spectrum contains a hint (at 1.9σ) of maser emission near −42.5 km s^{-1} with flux density around 0.2 Jy. The regular survey was not sensitive enough to confirm the detection. However, Voronkov et al. (2007) reported a convincing detection of the 104-GHz methanol maser in the source at the same velocity. The 104 and 9.9-GHz transitions belong to the same $(J + 1)_{-1}$ to J_{-2} E transition series ($J = 10$ and $J = 8$, respectively) and are expected to show similar behaviour. Therefore, it is likely that the 9.9-GHz maser is present in this source below the detection threshold of the survey. The flux density of the 9.9-GHz emission is at least an order of magnitude lower than might have been expected on the basis of

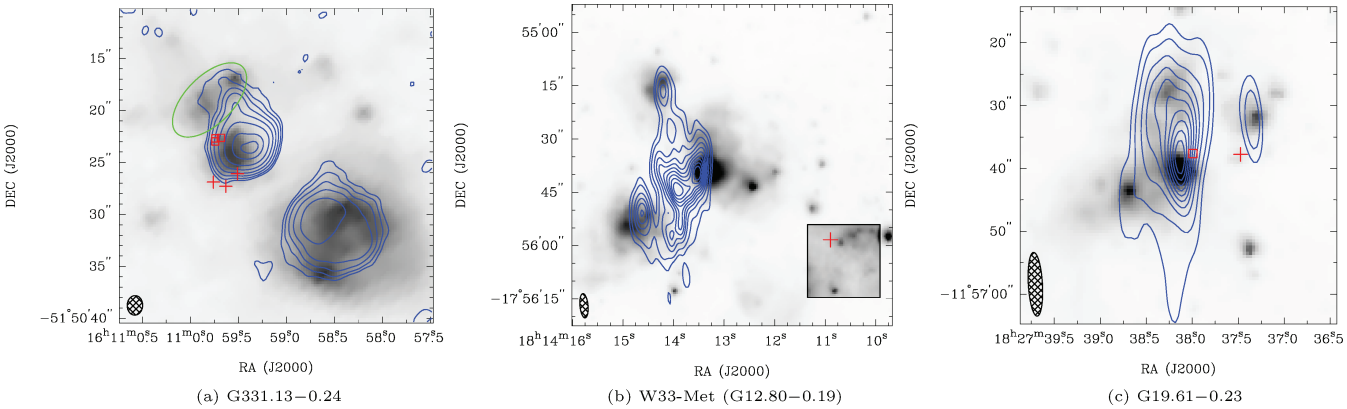

Figure 2. Radio continuum emission at 8.6 GHz (contours) in the vicinity of masers detected at 9.9 GHz overlaid on top of the *Spitzer* IRAC 4.5-μm image (grey-scale). The environment of G343.12−0.06 is shown in Fig. 3(a) and discussed in a separate paper (Voronkov et al. 2006). Position of the 6.7- and 9.9-GHz masers is shown by the open squares and crosses, respectively. (a) G331.13−0.24: the continuum image was obtained using the data of Phillips et al. (1998) to preserve high accuracy of the relative position of the 6.7-GHz maser with respect to the H II region. Contours are 1, 2, 4, 8, 16, 32, 64 and 90 per cent of 43 mJy beam^{-1}. The crosses represent three epochs of the measurement at 9.9 GHz, rather than individual maser spots. The ellipse represents the location of an EGO (Cyganowski et al. 2008). (b) W33-Met (G12.80−0.19): the 4.5-μm flux density has been multiplied by 10 inside the square in the bottom right-hand corner of the image. Contours are 5, 10, 20, 30, 40, 50, 60, 70, 80 and 90 per cent of 1.8 Jy beam^{-1}. (c) G19.61−0.23: contours are 5, 10, 20, 30, 40, 50, 60, 70, 80 and 90 per cent of 0.6 Jy beam^{-1}.

the only two other sources known to have both 104- and 9.9-GHz masers. Both G343.12−0.06 (Voronkov et al. 2006) and W33-Met (Voronkov et al. 2007) have flux densities at 104 GHz comparable with the 9.9-GHz ones reported in this paper (see Table 3). This most likely implies that markedly different physical conditions exist in this particular source. One may speculate that this might be related to another peculiarity found by Walsh et al. (2007): the high-mass star-forming region associated with G305B is bright in infrared, old according to the chemistry, but has no H II region sufficiently developed to be detectable. The expansion of an H II region could be hindered because of the dense environment and/or by continuing infall of the matter.

Voronkov et al. (2005a) detected a bright class I methanol maser at 25 GHz ($J = 5$ transition of the 25-GHz series) at −42.4 km s^{-1}, although without imaging and accurate flux density calibration. These masers have been shown to originate at the same spatial location as the 9.9-GHz maser in at least one source (Voronkov et al. 2006). An accurate position for the 25-GHz maser ($J = 4$ transition with the peak velocity of −42.1 km s^{-1} observed with the velocity resolution of 0.75 km s^{-1}) was determined by Walsh et al. (2007), but the reported flux density of the maser is much lower, due to insufficient spectral resolution. The 25-GHz maser was found to be 3 arcsec to the east from the position of the 6.7-GHz maser 305.202+0.208 (G305B region). It is worth noting that Walsh et al. (2007) also detected 25-GHz emission (several transitions of the series) towards two other locations in this source: near G305A and the south-eastern H II region. However, the radial velocity and a clear maser appearance of the feature near G305B allows an unambiguous identification of the suspected 9.9-GHz maser with this position, near the 6.7-GHz maser 305.202+0.208.

3.1.3 G331.13−0.24 detection

The 6.7-GHz masers in this source were mapped by Phillips et al. (1998) and found to be located near the edge of a 7 × 10 arcsec^2 H II region (see also Fig. 2a). According to Goedhart et al. (2004) this 6.7-GHz maser shows periodic flares with period around 500 d. The OH maser in the source is coincident with the cluster of the 6.7-GHz maser spots within the uncertainty of the absolute position measurement (Caswell 1998; Phillips et al. 1998). The 9.9-GHz maser is located close to the cluster of class II masers, but at a clearly distinct position. It is also seen projected on to the H II region but located near the edge. There is a protrusion in the image of the H II region near the location of the 9.9-GHz maser (Fig. 2a) indicating a possible interaction between expanding H II region and the surrounding material. The brightest 4.5-μm source within the boundaries of this H II region is located between the 6.7- and 9.9-GHz masers (Fig. 2a). Two weaker 4.5-μm sources surrounded by an extended emission are located near the northern tip of the H II region (as shown by an ellipse in Fig. 2a). This latter object has an excess of the 4.5-μm emission and is listed as an EGO by Cyganowski et al. (2008) despite being only a few seconds of arc across. The exact physical interpretation of this source is uncertain at present. However, considering its location it seems unlikely that this EGO could trace part of the shock front responsible for the 9.9-GHz maser.

De Buizer et al. (2009) mapped the SiO (2–1) emission towards G331.13−0.24 and detected an elongated SiO source with velocity gradient centred at the position of the 6.7-GHz masers with the axis roughly parallel with the east–west distribution of the 6.7-GHz maser spots. De Buizer (2003) reported the detection of a single knot of H_2 2.12-μm emission. This is located at the eastern edge of the redshifted SiO lobe (approximately 8 arcsec from the 6.7-GHz maser). Both these facts reveal pronounced shock activity in the region. However, the present data do not allow us to rule out the association of the 9.9-GHz maser with any certain structure seen in shock-tracing molecular emission as the spatial resolution of the SiO data is rather coarse and comparable to the separation between the 9.9- and 6.7-GHz masers.

3.1.4 G338.92−0.06, G339.62−0.12 and G9.62+0.20 non-detection

These sources were included in the target list as periodically variable 6.7-GHz masers (Goedhart et al. 2004), although Slysh et al. (1994) detected no class I maser emission at 44 GHz towards either of them.

Table 4. Sources without a 9.9-GHz detection. Flux density limit is 1σ. G329.031−0.19 and G329.029−0.20 represent two close positions within the same source.

Source name	Date of observations	Observed position α_{2000} (h m s)	Observed position δ_{2000} (° ′ ″)	Velocity range (km s^{-1})	Synthesized beam FWHM (arcsec)	Synthesized beam PA (°)	1σ image noise level (mJy beam^{-1})	1σ flux limit (mJy)	Separation from calibrator Angular (°)	Separation from calibrator Temporal (min)
G301.14−0.23	2005 December 15	12:35:34	−63:02:38	−97, −1	1.1 × 0.8	39	76	430	10.5	6.6 (1)
G305.21+0.21	2005 December 15	13:11:09	−62:34:41	−97, −1	1.1 × 0.8	33	82	470	14.5	6.9 (2)
G305.25+0.25	2005 December 15	13:11:33	−62:32:03	−97, −1	1.3 × 0.7	34	76	430	14.6	6.8 (2)
G305.36+0.20	2005 December 15	13:12:34	−62:33:25	−97, −1	1.3 × 0.7	35	81	460	14.7	17.2 (1)
G326.475+0.70	2005 December 15	15:43:17	−54:07:13	−94, +2	1.3 × 0.7	24	76	430	6.6	6.5 (1)
G326.641+0.61	2005 December 15	15:44:33	−54:05:29	−94, +2	1.3 × 0.8	26	69	390	6.5	6.4 (1)
G327.392+0.19	2005 December 16	15:50:18	−53:57:06	−124, −28	1.6 × 0.9	20	68	460	6.1	6 (1)
G326.859−0.67	2005 December 16	15:51:14	−54:58:05	−125, −29	1.6 × 1.0	9	89	610	5.2	5.4 (2)
G327.618−0.11	2005 December 16	15:52:50	−54:03:01	−124, −28	1.5 × 1.0	14	64	440	5.8	5.2 (1)
G327.29−0.58	2005 December 15	15:53:06	−54:37:06	−95, +1	1.3 × 0.7	25	62	350	5.3	6 (1)
G328.81+0.64	2005 December 15	15:55:48	−52:42:48	−94, +2	1.3 × 0.8	32	59	340	6.8	16 (3)
G328.237−0.54	2005 December 17	15:57:58	−53:59:23	−94, +2	1.2 × 0.8	−16	52	98	5.5	5.0 (1)
G329.469+0.50	2005 December 16	15:59:41	−52:23:28	−124, −28	1.5 × 1.0	14	61	410	6.9	5.3 (1)
G329.031−0.19	2005 December 17	16:00:30	−53:12:27	−94, +2	1.2 × 0.8	−14	52	98	6.1	4.9 (1)
G329.029−0.20	2005 December 17	16:00:32	−53:12:50	−94, +2	1.2 × 0.9	−12	52	98	6.1	4.9 (1)
G329.066−0.30	2005 December 17	16:01:10	−53:16:03	−94, +2	1.2 × 0.8	−11	53	100	6.0	4.9 (1)
G329.183−0.31	2005 December 17	16:01:47	−53:11:44	−94, +2	1.1 × 0.9	−3	52	98	6.0	5 (1)
G331.442−0.18	2005 December 16	16:12:12	−51:35:10	−124, −28	1.8 × 0.9	16	51	350	7.3	7 (3)
G331.342−0.34	2005 December 16	16:12:26	−51:46:17	−124, −28	1.5 × 0.9	36	61	410	7.1	5.3 (1)
G332.295−0.09	2005 December 17	16:15:45	−50:55:54	−94, +2	1.1 × 0.9	34	52	98	7.9	5.3 (8)
G332.604−0.16	2005 December 17	16:17:29	−50:46:13	−93, +3	1.2 × 0.8	−7	53	100	8.0	5.0 (1)
G333.029−0.06	2005 December 17	16:18:57	−50:23:54	−93, +3	1.2 × 0.9	−9	52	98	8.4	5.0 (1)
G333.315+0.10	2005 December 17	16:19:29	−50:04:41	−93, +3	1.2 × 0.9	−8	52	98	8.7	5.0 (1)
G333.184−0.09	2005 December 16	16:19:46	−50:18:35	−124, −28	1.7 × 1.0	29	57	390	8.5	5.0 (5)
G333.163−0.10	2006 March 25	16:19:43	−50:19:53	−136, −40	1.3 × 0.7	5	61	76	4.9	5.3 (1)
G333.23−0.05	2005 December 16	16:19:48	−50:15:02	−124, −28	1.8 × 1.0	20	54	370	8.6	5 (1)
G333.121−0.43	2005 December 17	16:21:00	−50:35:52	−94, +3	1.1 × 0.9	34	49	92	8.2	5.0 (1)
G333.562−0.02	2005 December 17	16:21:09	−49:59:48	−93, +3	1.2 × 0.9	−3	52	98	8.8	5 (1)
G332.942−0.69	2005 December 17	16:21:19	−50:54:10	−94, +2	1.1 × 0.9	29	49	92	7.9	5.3 (5)
G333.466−0.16	2006 March 25	16:21:20	−50:09:49	−105, −9	1.3 × 0.7	8	60	75	4.6	5.2 (1)
G332.963−0.68	2006 March 25	16:21:23	−50:52:59	−106, −10	1.3 × 0.7	9	61	76	4.6	13.9 (1)
G333.130−0.56	2006 March 25	16:21:36	−50:40:51	−106, −10	1.4 × 0.7	12	61	76	4.5	5.2 (1)
G335.060−0.42	2006 March 26	16:29:23	−49:12:27	−75, +22	1.5 × 0.7	19	57	71	3.7	5.4 (1)
G337.40−0.41	2006 March 25	16:38:50	−47:28:18	−103, −7	1.4 × 0.7	9	61	76	3.8	5.1 (1)
G338.92+0.56	2005 December 16	16:40:32	−45:41:53	−123, −27	2.0 × 0.9	8	50	340	13.6	5.7 (3)
G338.92−0.06	2006 March 25	16:43:16	−46:05:42	−102, −6	1.4 × 0.7	9	61	76	4.8	13.8 (1)
G339.62−0.12	2006 March 26	16:46:05	−45:36:43	−72, +24	1.6 × 0.7	17	57	71	5.2	5.6 (1)
G345.01+1.79	2006 March 26	16:56:49	−40:14:20	−69, +27	1.7 × 0.7	16	58	73	10.6	5.9 (3)
G345.00−0.22	2006 March 26	17:05:10	−41:29:04	−69, +27	1.7 × 0.7	16	58	73	9.6	15.2 (3)
G351.16−0.70	2006 March 26	17:19:57	−35:57:46	−66, +30	1.9 × 0.7	15	58	73	9.1	6.0 (6)
G351.24+0.67	2006 March 25	17:20:16	−35:54:58	−24, +46	1.4 × 1.0	30	62	78	9.0	5.5 (3)
G351.41+0.64	2006 March 26	17:20:53	−35:47:02	−66, +30	1.9 × 0.7	15	58	73	8.9	5.9 (4)
G351.78−0.54	2006 March 26	17:26:43	−36:09:18	−66, +30	1.8 × 0.7	16	57	71	9.6	5 (1)
G0.54−0.85	2006 March 25	17:50:15	−28:54:51	−32, +64	1.7 × 1.0	23	60	75	8.3	14.5 (5)
G9.621+0.196	2006 March 26	18:06:15	−20:31:32	−60, +37	3.0 × 0.7	9	58	73	13.7	16 (1)
G18.34+1.77	2006 March 25	18:17:57	−12:07:22	−28, +68	3.7 × 1.1	7	61	76	11.0	13 (3)

Kurtz et al. (2004) found weak 44-GHz maser emission towards G9.62+0.20, which was below the detection threshold of Slysh et al. (1994). Despite the fact that we observed all three sources in a good weather providing a 1σ flux density limit of around 70–80 mJy (see Table 4), no emission at 9.9 GHz was detected.

3.1.5 G343.12−0.06 (IRAS 16547−4247) detection

The 9.9-GHz maser was discovered in this source during the pilot survey. It has been investigated in detail in a separate paper (Voronkov et al. 2006) and is included here for completeness. The maser is associated with the brightest knot of the H_2 emission (Brooks et al. 2003) tracing an outflow (see Fig. 3a; Voronkov et al. 2006). This particular location is the only place where the 25- and 104-GHz masers were detected in this source, in contrast to the widespread class I methanol masers detected in a number of maser spots (Voronkov et al. 2006). Garay et al. (2003) first detected cm-wavelength continuum emission in the source comprising a brighter central object and two weaker satellites (further resolved by Rodríguez et al. 2005). The central object and the satellites were interpreted as thermal (free–free) emission from a radio jet and internal working surfaces of the jet, respectively. The 12-mm

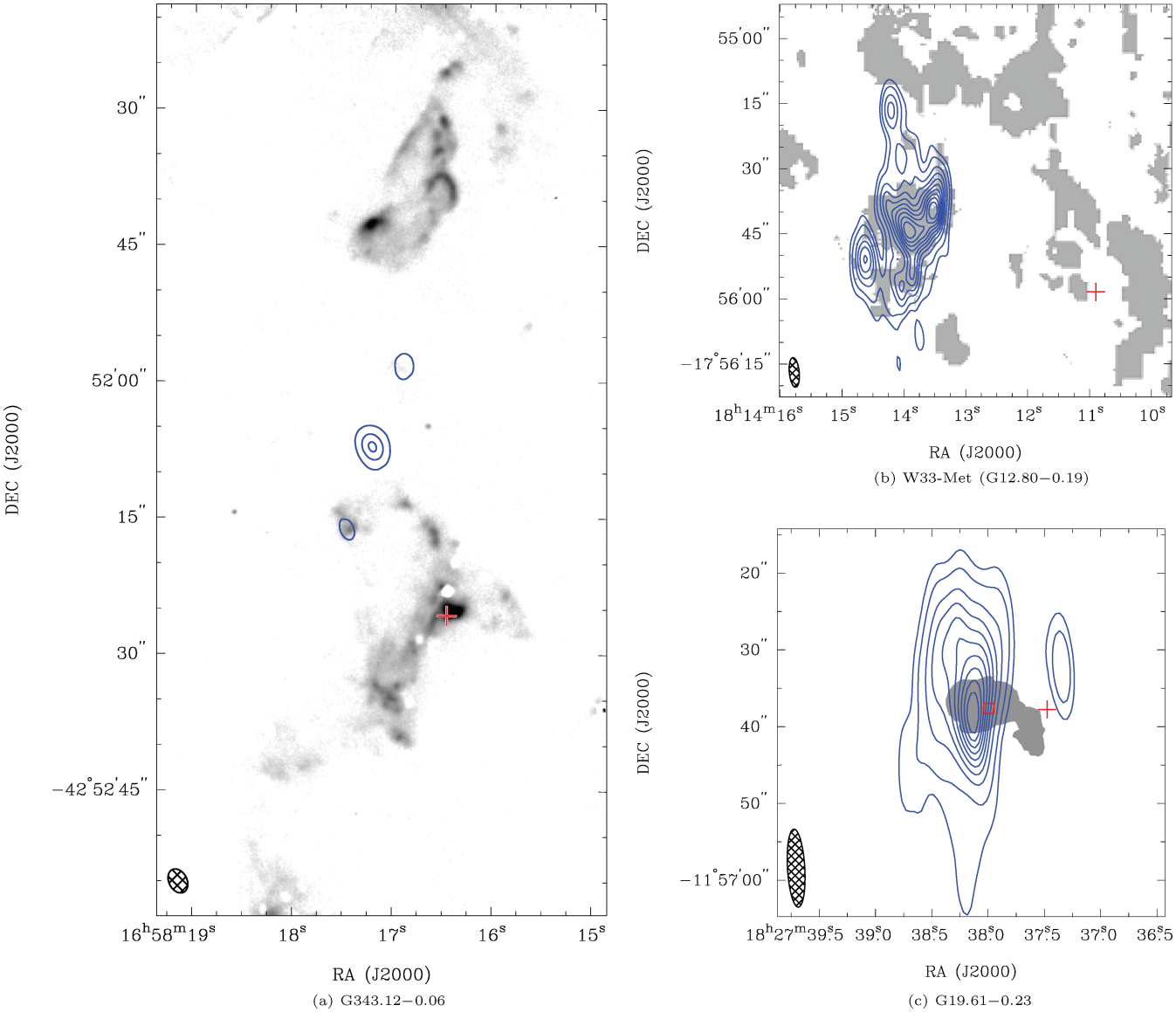

Figure 3. Association of the 9.9-GHz masers with outflow and hot molecular gas in the vicinity of H II regions. Position of the 9.9-GHz masers is shown by crosses and the 6.7-GHz maser in just G19.61−0.23 by an open square. (a) G343.12−0.06: the maser position is overlaid on top of the H_2 2.12-μm emission (Brooks et al. 2003) and the 12-mm continuum (Voronkov et al. 2006) showing an association with outflow. Contours are 15, 50 and 90 per cent of 13 mJy beam^{-1}. (b) W33-Met (G12.80−0.19): the grey-scale shows the (1, 1) ammonia emission (Keto & Ho 1989). Contours show the 8.6-GHz continuum as in Fig. 2(b). (c) G19.61−0.23: the grey-scale represents the (2, 2) ammonia emission from Garay et al. (1998). The northern molecular clump seen in absorption is not shown in this figure. Contours show the 8.6-GHz continuum as in Fig. 2(c).

image of these continuum sources from Voronkov et al. (2006) is shown in Fig. 3(a) along with the 2.12-μm molecular hydrogen image (Brooks et al. 2003) and the 9.9-GHz maser position. Forster & Caswell (1989) detected mainline OH masers at a position close to the central continuum source (Fig. 3a). No 6.7-GHz emission has been detected with an upper limit of 0.3 Jy (Caswell et al. 1995; Walsh et al. 1998).

3.1.6 G351.16−0.70, G351.24+0.67 and G351.41+0.64 non-detection

These are the positions within NGC 6334 complex, one of the most prominent sites of massive-star formation. They correspond to sources V, IV and I/I(N), respectively (see e.g. Muños et al. 2007, and references therein). The massive twin cores NGC 6334I and I(N) have been studied for more than two decades and are believed to be at different evolutionary stages (see Beuther et al. 2008, and references therein). These cores are well known to host unusual methanol masers of both classes (e.g. Menten & Batrla 1989; Cragg et al. 2004; Ellingsen et al. 2004). There are class II methanol masers at 6.7 GHz associated with both cores (Walsh et al. 1998), but the maser in the core I is one of the brightest known 6.7-GHz masers of more than 3000 Jy. In contrast, the northern core, I(N), is remarkable in its class I maser emission (e.g. Brogan et al. 2009). Although both sites emit at 25 GHz, it is likely to be a maser in the I(N), while source I is responsible for quasi-thermal emission (Menten & Batrla 1989; Haschick et al. 1990; Beuther et al. 2005). No 9.9-GHz maser emission has been detected towards either of these positions with the 1σ flux density limit of 70–80 mJy.

3.1.7 W33-Met (G12.80−0.19) detection

The W33 region, which hosts a cluster of young massive stars, is renowned for its strong radio continuum emission and a complex molecular environment (Goss, Matthews & Winnberg 1978; Goldsmith & Mao 1983; Ho, Klein & Haschick 1986). The first detection of a methanol maser towards this source was reported by Menten et al. (1986). They observed a number of class I maser transitions of the 25-GHz series and revealed a positional offset of the masers with respect to the dominant continuum source. The 44-GHz methanol masers were later found in the vicinity of this offset position by Haschick et al. (1990), who introduced the notation W33-Met to distinguish methanol maser site from the main continuum source in the region. Before we started the project, this was the only source known to have a 9.9-GHz maser (Slysh et al. 1993). Although our measurement gives the peak flux density as 4.3 Jy, Slysh et al. (1993) reported just 0.8 Jy. Partially, this is the result of the 2.5 times lower spectral resolution in the Slysh et al. (1993) data, as the line is quite narrow (Fig. 1). However, the spectral resolution alone cannot account for more than a factor of 4 difference in the flux density. It is not clear how accurate the absolute flux scale calibration was for the Slysh et al. (1993) single-dish data, especially given the strong cm-wavelength continuum in the source. Therefore, we do not draw any conclusions from this discrepancy, although temporal variability cannot be excluded. Slysh et al. (1993) reported the peak velocity of the maser at 33.5 km s^{-1}, which is notably different from 32.72 km s^{-1} obtained in our measurement (Table 3) even taking into consideration the spectral resolution achieved in both experiments. However, this discrepancy can be explained by the less accurate value of the rest frequency used by Slysh et al. (1993) to calculate the radial velocities. The difference in adopted rest frequencies accounts for 0.85 km s^{-1} of the velocity offset, bringing the radial velocity into agreement within the spectral resolution. The radial velocity of the 9.9-GHz maser is also in agreement with the velocity of the 25-GHz masers reported by Menten et al. (1986), provided the rest frequency adopted by Menten et al. (1986) is more accurate than the spectral resolution of their measurement.

The continuum source has a complex structure reflecting the presence of multiple young stars (Fig. 2b). The morphology is in general agreement with the earlier results of Ho et al. (1986), but the 1.5-GHz emission (20 cm) is extended more to the west than the emission at higher frequencies. This is most obvious if one compares the association between the (1, 1) inversion transition of ammonia and the rim of the 1.5-GHz emission depicted by Keto & Ho (1989) in their fig. 2 with Fig. 3(b) in this paper, where the same ammonia distribution from Keto & Ho (1989) is overlaid on top of the 8.6-GHz continuum from our observations. Fig. 3(b) clearly shows a gap of around 15 arcsec between the 8.6-GHz continuum source and the ridge of ammonia emission. As concluded by Ho et al. (1986), the smooth emission filling the gap is most likely resolved at higher frequencies. According to the interpretation of Keto & Ho (1989) the ridge of ammonia emission is due to shocks caused by interaction of the ionized gas with the neutral component. The 9.9-GHz maser is located near the western clump of the ammonia emission (Fig. 3b). This position is in agreement with the position of the 25-GHz masers reported by Menten et al. (1986) within the uncertainty of their measurement.

The *Spitzer* IRAC image revealed a number of 4.5-μm sources associated with some of the continuum peaks (see Fig. 2b). There is an extended 4.5-μm emission located largely near the western edge of the 8.6-GHz continuum source in the area where the continuum emission has been detected at 1.5 GHz only. The inspection of other IRAC bands revealed no significant excess of the 4.5-μm emission, which is in agreement with this object not being listed as an EGO by Cyganowski et al. (2008). However, it is worth noting that there is a faint compact 4.5-μm source located just 3 arcsec to the west of the 9.9-GHz maser position. This infrared source is detected in the 4.5-μm IRAC band only.

Although Menten (1991) reported the detection of the 6.7-GHz maser in W33-Met, a comparison of the velocity range with the source G12.91−0.26 reported by Caswell et al. (1995) suggests possible confusion. We processed archival ATCA data (project code C415) using the standard reduction technique and found two 6.7-GHz masers G12.68−0.18 ($\alpha_{2000} = 18^{\rm h}13^{\rm m}54\overset{\rm s}{.}74 \pm 0\overset{\rm s}{.}01$, $\delta_{2000} = -18^{\circ}01'46\overset{''}{.}1 \pm 0\overset{''}{.}1$) and G12.91−0.26 ($\alpha_{2000} = 18^{\rm h}14^{\rm m}39\overset{\rm s}{.}52 \pm 0\overset{\rm s}{.}02$, $\delta_{2000} = -17^{\circ}51'59\overset{''}{.}1 \pm 0\overset{''}{.}2$), situated 7.0 and 7.9 arcmin away from the 9.9-GHz methanol maser position, respectively. The 1σ rms noise level at the position of the 9.9-GHz maser at 6.7 GHz is 0.1 Jy. Caswell (2009) provided an independent position measurement of the confusing 6.7-GHz masers which agrees well with the values given above.

3.1.8 G18.34+1.77 (IRAS 18151−1208) non-detection

Although the widespread class I maser transitions (e.g. at 44 GHz) are not atypical in this source, it has one of the brightest 25-GHz methanol masers found outside Orion and NGC 6334 (the $J = 5$ maser peaks at +29.7 km s^{-1} and has a flux density exceeding 15 Jy, Voronkov et al., unpublished observations). Davis et al. (2004) detected two H_2 outflows in this source which could be related to the 25-GHz masers. High angular resolution observations are required to confirm this. No 9.9-GHz maser emission has been detected in this source with the 1σ flux density limit of 76 mJy, which implies that the flux density of the 25-GHz maser exceeds that of the 9.9-GHz maser by at least two orders of magnitude.

3.1.9 G19.61−0.23 detection

This region hosts a cluster of young high-mass stars and is somewhat similar in appearance to W33-Met at cm wavelength (Figs 2b and c), albeit with a smaller angular separation between components. Furuya et al. (2005) identified nine ultracompact H II regions and a hot core squeezed between two of them designated A and C. The 8.6-GHz continuum image (Fig. 2c) obtained in our survey qualitatively agrees with the results of Furuya et al. (2005), although the elongated beam does not allow us to disentangle close components easily. A number of continuum peaks coincide with the 4.5-μm emission from the *Spitzer* IRAC image (see Fig. 2c). The brightest 4.5-μm source is associated with the most prominent H II region (labelled A in Furuya et al. 2005). This source is not listed as an EGO by Cyganowski et al. (2008).

The hot core is responsible for emission in a number of molecular species (Furuya et al. 2005; Wu et al. 2009) and is associated with the brightest ammonia clump (named middle clump) found by Garay et al. (1998). Garay et al. (1998) identified two more ammonia clumps: the northern clump seen in absorption and the elongated south-western clump seen in emission. The relative position of the 8.6-GHz continuum, ammonia emission (from Garay et al. 1998, absorption source is not shown) and the 9.9-GHz maser is shown in Fig. 3(c). The 9.9-GHz maser is located near the elongated south-western clump, which Garay et al. (1998) interpreted as arising from the compressed and heated gas behind the shock front driven by the expansion of the largest H II region in the source. Kurtz et al. (2004)

observed this source at 44 GHz and revealed two maser spots. The brightest 44-GHz spot is colocated both in position and velocity with the 9.9-GHz maser within the combined error of the measurements. The weaker feature peaks at 46.5 km s^{-1}. It corresponds to a maser spot located 7.9 arcsec to the north-east from the brightest spot (and the 9.9-GHz maser spot) roughly along the ammonia filament.

Caswell et al. (1995) detected a weak 6.7-GHz methanol maser with a peak flux density of 0.4 Jy in this source. This maser is located 7.6 arcsec away from the position of the 9.9-GHz maser, at $\alpha_{2000} = 18^{\rm h}27^{\rm m}37\overset{\rm s}{.}993 \pm 0\overset{\rm s}{.}006$, $\delta_{2000} = -11^{\circ}56'37\overset{''}{.}6 \pm 0\overset{''}{.}4$ (Caswell, unpublished observations). The position suggests an association of this maser with the hot core and the middle ammonia clump (see Fig. 3c). Garay, Reid & Moran (1985) found a number of OH maser spots clustered near the 6.7-GHz maser position and also associated with the middle ammonia clump (see also Forster & Caswell 1989).

4 DISCUSSION

4.1 Temporal variability of G331.13−0.24

Inspection of the three epochs listed in Table 3 suggests possible temporal variability of the 9.9-GHz maser in G331.13−0.24, with the caveat that the only measurement which stands out significantly was taken under imperfect weather conditions. The variability of the class I methanol masers is not well understood at the moment. However, the class II maser at 6.7 GHz in this source is known to be somewhat exceptional. This is one of the seven periodically variable masers known to date (Goedhart et al. 2004), which has the longest period in the sample of around 500 d. The coexistence of 6.7- and 9.9-GHz masers in this source is a unique situation with great potential to shed light on the nature of periodic flares because these two transitions are predicted to react in opposite ways to the changes in pumping. The pumping mechanisms of these two maser transitions are in conflict as they belong to different classes. Hence, if the flares occur due to a pumping variation of any nature, the intensity variations in the two transitions are expected to anticorrelate. On the other hand, both masers are seen projected towards the same H II region. This means that this H II region provides the seed radiation which both masers amplify. If the variations are due to changes in the seed radiation, intensity variations in the two transitions will correlate. Thus simple monitoring of the 9.9-GHz maser may unravel a vital aspect of the flare mechanism. We have started such a project and will report the results elsewhere.

The main complication arises from the fact that class I and class II masers are not colocated. In this and some other periodically variable sources, flares of the different 6.7-GHz spectral features, which are presumably also separated in space, are delayed with respect to each other, sometimes by up to a few weeks (Goedhart et al. 2004). Although the velocity of the 9.9-GHz maser is close to the velocity of one of the groups of the 6.7-GHz maser lines, the angular separation is an order of magnitude greater than the size of the 6.7-GHz cluster. Therefore, a longer delay of the order of months is quite possible. The 9.9-GHz flux measurements presented in this paper all correspond to the descending part of the 6.7-GHz light curve, approximately 20, 4 and 10 weeks after the maximum (Goedhart et al., unpublished recent monitoring data), respectively, for each epoch listed in Table 3. Although this is consistent with the steady fall of the 9.9-GHz flux density along with the 6.7-GHz flux density, a longer time-series is required to obtain a definitive answer. The long period of around 500 d as well as the non-sinusoidal shape of the light curve (see Goedhart et al. 2004) will help to distinguish between a possible delay and anticorrelation in this particular source.

Monitoring of the masers has a number of advantages over monitoring the continuum emission directly. First, the masers amplify the continuum and so essentially undetectable variations of the continuum flux can cause significant variations in the maser intensity. Secondly, the continuum source has a complex shape in G331.13−0.24 making it very difficult to undertake accurate flux density monitoring as it is hard to reproduce exactly the same uv coverage in all epochs. In contrast, each spectral feature of the methanol maser corresponds to a point source for the baselines of the order of a few kilometres long, making flux monitoring a much easier task. It is worth noting that there is an agreement to better than 2 per cent (which is likely to be the limit of the absolute flux density calibration) between the flux density of the H II region measured by Phillips et al. (1998) and that obtained in this paper.

4.2 Coexistence with class II methanol masers at 6.7 GHz

As was mentioned above, our target list comprised largely known class I methanol masers. The majority of these class I masers were found towards known 6.7-GHz masers (class II), as they are often located within the beam of the single dish used for class I measurements (e.g. Slysh et al. 1994; Ellingsen 2005). The remaining sources were either well-known star-forming regions (e.g. positions within the NGC 6334 complex) or were found towards known H_2O masers (e.g. Bachiller et al. 1990), H II regions or main-line OH masers (e.g. Slysh et al. 1994). Despite being selected by other criteria many of the sources from the second group also have a 6.7-GHz methanol maser in the vicinity. Therefore, only one target in our sample, W33-Met, has a class I methanol maser without a 6.7-GHz counterpart. Another such source is G343.12−0.06 (Voronkov et al. 2006).

In total, out of four 9.9-GHz methanol masers currently known, two do not have a 6.7-GHz counterpart detected, and one source, G19.61−0.23, has a very weak 6.7-GHz maser. The fourth source, G331.13−0.24, has both masers projected on to an H II region, a situation favouring detection of low-gain masers. These results suggest that the 9.9-GHz masers tend to be associated with sources with class I masers without strong class II counterparts. A proper statistical test is not yet possible due to a small number of known 9.9-GHz masers. However, a number of previous studies have already investigated relations between the widespread class I masers (e.g. at 44 or 95 GHz) and the class II masers at 6.7 GHz (e.g. Slysh et al. 1999; Ellingsen 2005). Slysh et al. (1999) were motivated by the conflicting pumping mechanisms of these masers, although the present data suggest that the class I and class II masers are rarely seen at the same location at high spatial resolution (e.g. Kurtz et al. 2004; Cyganowski et al. 2009). The exceptions are probably due to the projection effect, although unusual pumping under common conditions (e.g. Voronkov et al. 2005b) cannot be excluded. Therefore, any tendency (e.g. for bright masers of one class to avoid the bright masers of another class), if present, is likely to be related to the general trends in the distribution of the physical parameters affecting the pumping across the star-forming region, rather than the conditions at any single location in the source. These trends can be idiosyncratic to some extent due to the complex structure of high-mass star-forming regions (e.g. one region could be more embedded in the parent molecular cloud than another). However, they can also change during the course of evolution, for example when an outflow turns on or an H II region starts to expand. It is worth noting that using a statistically complete sample of sources,

Ellingsen (2005) found no evidence for the original anticorrelation between flux densities reported by Slysh et al. (1999). However, the 9.9-GHz masers require a more restrictive range of physical conditions (e.g. temperature and density) to appear than the widespread class I methanol masers at 44 and 95 GHz. It is therefore possible that the anticorrelation with the 6.7-GHz masers is more pronounced for these 9.9-GHz masers than for the widespread 44 and 95-GHz ones.

4.3 Association with expanding H II region

Out of 48 sources searched for the 9.9-GHz emission in this paper (note that G329.031−0.19 and G329.029−0.20 are counted as a single source), 35 sources have 8.6-GHz continuum sources, presumably H II regions, within the primary beam (half-power width is about 5 arcmin) and 13 sources do not (1σ rms noise level not corrected for decorrelation and primary beam attenuation is about 0.3 mJy). Three of these continuum sources correspond to periodically variable 6.7-GHz masers and two of them do not have class I methanol masers detected so far in any transition. Even allowing for a few confused cases due to a large beam (most known class I masers have single-dish positions), our target sample, comprising largely known class I masers at 44 and 95 GHz, appears to be biased to some extent towards the star formation sites with H II regions. The present data do not yet allow us to establish reliably whether the common occurrence for class I masers to have an H II region in the vicinity has physical significance or is just a selection effect. In contrast, it is well established that only a small fraction of class II methanol masers at 6.7 GHz are associated with detectable H II regions (e.g. Walsh et al. 1998).

All four currently known 9.9-GHz maser sources have a cm-wavelength continuum detected in the vicinity of the maser spot. Three masers found in the regular survey are located in close proximity to well-developed H II regions (Fig. 2). While the remaining source, G343.12−0.06, is renowned for thermal emission from the jet driving an outflow (Fig. 3a; Brooks et al. 2003; Voronkov et al. 2006). As mentioned in Section 3.1, in some cases the molecular emission could arise due to interaction between ionized and neutral material. Such an interpretation has been suggested on the basis of kinematics and morphology for at least two sources, W33-Met and G19.61−0.23 (Keto & Ho 1989; Garay et al. 1998). The expansion of an H II region drives shocks into the surrounding molecular cloud heating and compressing the gas. It is this change in the physical conditions which is most likely traced by the ammonia emission (Figs 3b and c). In both W33-Met and G19.61−0.23, the 9.9-GHz maser is located just beyond the edge of the ammonia source, further away from the H II region which is believed to be undergoing expansion. The separation between the maser and the nearest ammonia emission is of the order of a few seconds of arc. Although the magnitude of this separation could probably be explained by the combined accuracy of the absolute positions, the picture agrees well with the basic expectation that a more fragile molecule like methanol should be located predominantly further away from the exciting source than ammonia.

Kirsanova, Wiebe & Sobolev (2009) modelled the expansion of an H II region surrounded by molecular gas and demonstrated formation of a transition layer characterized by high abundance of molecules in the gas phase. The location and thickness of this transition layer vary from molecule to molecule and also depend on the initial temperature and density of the quiescent gas. Although the methanol chemistry was not modelled by Kirsanova et al. (2009), the physical conditions in the transition layer, such as temperature and density, simulated in these models could clearly be in the range suitable for the formation of class I masers (e.g. Voronkov et al. 2005b).

The geometry of G331.13−0.24 and the data on the thermal molecular environment available for this source do not allow us to make conclusions about the nature of the 9.9-GHz maser. As previously mentioned in Section 3.1, there is an SiO emission (presumably tracing shocks) detected in this source (De Buizer et al. 2009) at a position which does not allow us to completely rule out the association with the maser. On the other hand, the 9.9-GHz maser is located near the protrusion on the southern side of the H II region (see Fig. 2a) which may reflect the presence of the same type of interaction between the ionized and neutral material as described above. Although the remaining source G343.12−0.06 is a clear case where the 9.9-GHz maser is associated with an outflow (Fig. 3a; Voronkov et al. 2006), these considerations show that the outflow scenario may not be the only option.

This idea should equally apply to other class I masers, including 36- and 44-GHz ones, which are more ubiquitous than the 9.9-GHz masers. Therefore, future interferometric surveys of class I masers, e.g. a follow-up of the MMB survey (briefly mentioned in Caswell et al. 2010), have a great potential to test this hypothesis. It is worth mentioning that Kogan & Slysh (1998) observed W33-Met at 44 GHz. However, phase referencing was not used in their experiment making the search for possible associations difficult due to a lack of absolute positions.

4.4 Evolutionary stages

The question whether different masers trace distinct evolutionary stages of high-mass star formation has been investigated for more than two decades (e.g. Forster & Caswell 1989; Codella & Moscadelli 2000; Ellingsen 2005, 2006; Voronkov et al. 2006; Breen et al. 2010). The majority of class II methanol masers at 6.7 GHz are associated with millimetre and submillimetre sources (Walsh et al. 2003; Hill et al. 2005), while only a small fraction shows association with detectable H II regions (Phillips et al. 1998; Walsh et al. 1998). This leaves no doubt that they trace a very early stage of the (proto)stellar evolution preceding the formation of an H II region, and fade out shortly after an H II region forms. Breen et al. (2010) find that the other widespread class II methanol masers at 12.2 GHz most likely lag behind the 6.7-GHz masers. The latter seem to largely overlap with the H_2O masers (Szymczak, Pillai & Menten 2005) whereas the OH masers are usually considered to be a signature of a somewhat more evolved stage since they show a greater overlap with the ultracompact H II regions than is typical for class II methanol masers (Forster & Caswell 1989; Caswell 1997).

However, it is still poorly understood as to where the class I methanol masers fit into this picture. The main obstacle is the lack of unbiased surveys of the class I masers, which cover a substantial part of the Galaxy. As discussed above, the majority of currently known class I methanol masers have been found in surveys targeted towards class II methanol masers. Therefore, the sample of currently known class I masers is strongly biased towards the evolutionary stage traced by the 6.7-GHz masers. Without a widespread and bright low-frequency class I methanol maser transition (similar to the class II maser transition at 6.7 GHz or mainline OH) a blind survey is very time consuming. Therefore, Pratap et al. (2008) adopted an interesting strategy to cover several known molecular clouds in their, otherwise untargeted, search for class I methanol masers at 36 and 44 GHz. Comparison with the presence of H II regions and infrared sources, led Pratap et al. (2008) to suggest that the 36-GHz

masers may appear earlier than the 44-GHz masers during the evolution of a star-forming region. However, these data do not allow interrelations between evolutionary stages where the class I and class II methanol masers are present to be established. Ellingsen (2006) investigated this question using the infrared properties of a subsample of methanol masers associated with GLIMPSE (Galactic Legacy Infrared Mid-Plane Survey Extraordinaire) catalogue point sources. It was found that the sources with a class I maser seem to have redder GLIMPSE colours than those without it. With the caveat that the small number statistics made any firm conclusion impossible, Ellingsen (2006) suggested that the class I methanol masers may signpost an earlier stage of high-mass star formation than the class II masers.

These and other considerations led Ellingsen et al. (2007) to propose a qualitative evolutionary scheme for the different maser transitions, which has subsequently been further refined by Breen et al. (2010) in their fig. 6. In this sequence the class I masers represent the first signatures of high-mass star formation and fade out within approximately 2×10^4 yr after the onset of the 6.7-GHz maser emission. Based on the detailed study of G343.12−0.06, Voronkov et al. (2006) pointed out that the suggestion that class I methanol masers precede class II is inconsistent with the presence of OH masers and the lack of the 6.7-GHz maser emission in this source. OH maser emission in the absence of 6.7-GHz masers is more consistent with an evolved stage of star formation (see e.g. Caswell 1997).

It is important to keep in mind the major assumptions which underlie the evolutionary timeline put forward by Ellingsen et al. (2007) and Breen et al. (2010). In particular, that each major maser species arises only once during the evolution of a particular star formation region, and that all the maser species are associated with a single astrophysical object. For regions where the positions of the different maser species are known to an accuracy of 1 arcsec or better this latter assumption can be proven or disproved for most transitions; however, the larger spatial (and angular) scale over which class I methanol masers are often observed makes it much less clear whether the emission is due to a single object (see e.g. Kogan & Slysh 1998; Kurtz et al. 2004; Voronkov et al. 2006; Cyganowski et al. 2009). The degree of overlap of the class I and class II methanol masers on the timeline of Ellingsen et al. (2007) and Breen et al. (2010) is based on the rate of detection of class I methanol masers towards class II masers observed by Ellingsen (2005). However, the idea that class I methanol masers precede the class II was based purely on the circumstantial evidence that the former are associated with outflows, which are generally considered to be signposts of young objects, and the suggestion of Ellingsen (2006) that the class I masers may be associated with redder GLIMPSE point sources. As discussed earlier, all the 9.9-GHz masers found in this paper are located near H II regions (see Section 4.3), all but W33-Met have OH masers detected (see Section 3.1; no sensitive OH data seem to be available for W33-Met) and one source, W33-Met, does not have a 6.7-GHz maser detected (see Section 4.2). Despite the small number of sources, these similarities encourage us to revisit the question of where class I methanol masers fit into a maser-based evolutionary sequence.

Contrary to the sequence presented by Breen et al. (2010) it is clear that class I masers do overlap in time with OH masers. The 9.9-GHz maser detections reported in this paper reinforce the conclusion, although the class I masers in other transitions were already known for all of these sources (e.g. Bachiller et al. 1990; Slysh et al. 1994; Liechti & Wilson 1996). Despite the biased target selection in the majority of class I maser surveys, a few sources such as W33-Met (see Section 3.1) and G343.12−0.06 (Voronkov et al. 2006), are known to have class I masers without a class II counterpart at 6.7-GHz (see also Section 4.2). This suggests that it is more appropriate to place the class I methanol masers as partly overlapping, but largely post-dating the evolutionary phase associated with class II methanol masers. As a part of the follow-up programme based on the MMB untargeted survey briefly mentioned by Caswell et al. (2010), class I methanol masers at 44 GHz were searched for towards a number of OH masers which have no detected 6.7-GHz masers. The full results of this work will be reported elsewhere. However, the preliminary analysis indicates a detection rate greater than 50 per cent. This supports the hypothesis on the lifetime of class I masers given above and moreover suggests that the result is not unique for the 9.9-GHz masers and also applies to the widespread class I methanol masers (e.g. that at 44 GHz).

The class I masers are formed in moderately dense gas separated from strong infrared sources (for discussion, see e.g. Voronkov et al. 2006). These masers have radial velocities close to that of a parent molecular cloud which suggests, together with morphology, an association with the interface region. Weak shocks interacting with the molecular cloud dramatically change the chemical composition of the medium by releasing methanol and other complex molecules from the dust grain mantles into the gas phase. This increase of methanol abundance is observed in the shock-processed regions related to outflows (e.g. Gibb & Davis 1998). However, the same effect is also expected if other mechanisms, not just outflows, drive shocks into the parent molecular cloud, provided the shocks are weak enough and do not dissociate methanol molecules. In particular, as discussed in Section 4.3, class I methanol masers could be associated with expanding H II regions as well as with outflows. The presence of an H II region implies that the star formation in a particular site is quite evolved. On the other hand, an ample amount of molecular material interacting with an outflow or expanding H II region is required to produce a detectable maser. Therefore, there could be a bias towards deeply embedded regions of star formation. The amount of quiescent material remaining in a star-forming region showing maser activity depends not only on the age, but also on the initial conditions which may vary from one site to another.

It important to recall that high-mass star formation usually occurs in a crowded environment where sequential or triggered star formation may take place. G19.61−0.23 and W33-Met are good examples of clustered star formation. For example, Ho et al. (1986) suggested that the interaction of ionized gas from an earlier epoch of star formation may have triggered the formation of a second generation stars in W33-Met through the radiation-driven implosion mechanism. Therefore, in some cases it may be impossible to attribute a class I maser spot to a particular YSO, especially taking into account that the angular offset of this maser may exceed the separation between YSOs in the cluster. In addition, the individual constituents of the cluster may have significantly different ages. For example, one YSO in the cluster may have an associated 6.7-GHz maser, while another could be associated with OH masers and a well-developed H II region. The fact that the class I methanol masers can be associated with both outflows and expanding H II regions, which presumably appear at different evolutionary stages, further complicates the situation. At this stage the number of sufficiently simple sources studied in detail is quite limited hindering the statistical analysis. The future interferometric surveys of the 44- and 36-GHz methanol masers (widespread class I maser transitions) will be vital for refining the evolutionary sequence for masers.

4.5 Association with the EGOs

Chen et al. (2009) found that approximately two-thirds of the EGOs from the list of Cyganowski et al. (2008), which have been observed at either 95 or 44 GHz, have a class I methanol maser detected within 1 arcmin. Based on this result, they made a comment that EGOs could be good targets for future class I maser searches. Such a survey of the 44-GHz masers carried out by Cyganowski et al. (2009) indeed had a high detection rate (90 per cent, 17 detections out of 19 EGOs observed). However, two out of four 9.9-GHz masers reported in this paper are not associated with an EGO (see Section 3.1). The physical nature of EGOs requires a better understanding (Cyganowski et al. 2009). One may speculate that the outflows are more likely to produce an EGO when they interact with the parent molecular cloud, than if shocks are caused by an expanding H II region. It is worth mentioning that the survey of Cyganowski et al. (2009) discovered an interesting class I methanol maser G49.27−0.34. No 6.7-GHz maser has been detected in this source (Cyganowski et al. 2009), while Mehringer (1994) detected smooth radio continuum from presumably a well-evolved H II region (seen at 20 cm only).

5 CONCLUSIONS

(i) Two new class I methanol masers at 9.9-GHz were found in addition to two other sources already reported in the literature. The absolute positions with arcsecond accuracy are summarized in Table 3 for all four 9.9-GHz masers known to date. Based on the trial observations, we also suspect that another 9.9-GHz maser may exist in G305.21+0.21 at a flux density below the detection threshold of our survey.

(ii) We suggest that some class I methanol masers may be associated with shocks driven into molecular cloud by an expanding H II region. This is an alternative scenario to the association with outflows which has been proved unambiguously in a number of other cases (e.g. Kurtz et al. 2004; Voronkov et al. 2006). This new scenario applies also to the class I methanol masers in other transitions, e.g. to the widespread masers at 36 and 44 GHz. It does not appear to be an exclusive mechanism to generate the 9.9-GHz masers, although it could be responsible for three out of four known 9.9-GHz masers.

(iii) The evolutionary stage with the class I maser activity is likely to outlast the stage when the 6.7-GHz methanol masers are present and overlap significantly in time with the stage when the OH masers are active. We expect that the class I masers in one of the widespread maser transitions (e.g. at 44 GHz) will be detected towards a significant number of OH maser sources which do not have a class II methanol maser at 6.7 GHz. Such sources were rarely observed in the class I maser surveys currently available in the literature.

(iv) A 9.9-GHz methanol maser was found in G331.13−0.24 which also hosts one of the few known periodically variable class II methanol masers at 6.7 GHz. This rare combination makes this source an attractive target for a long-term monitoring programme, which has a high potential to shed light on the periodic variability of masers.

ACKNOWLEDGMENTS

The Australia Telescope is funded by the Commonwealth of Australia for operation as a National Facility managed by CSIRO. SPE thanks the Alexander-von-Humboldt-Stiftung for an Experienced Researcher Fellowship which has helped support this research. AMS was financially supported by the Russian Foundation for Basic Research (grant 09-02-97019-a) and the Russian federal programme 'Scientific and scientific-pedagogical personnel of innovational Russia' (contracts N 02.740.11.0247 from 07.07.2009 and N 540 from 05.08.2009). This research has made use of NASA's Astrophysics Data System Abstract Service. This research has made use of data products from the GLIMPSE survey, which is a legacy science programme of the *Spitzer Space Telescope*, funded by the National Aeronautics and Space Administration. The research has made use of the NASA/IPAC Infrared Science Archive, which is operated by the Jet Propulsion Laboratory, California Institute of Technology, under contract with the National Aeronautics and Space Administration.

REFERENCES

Bachiller R., Menten K. M., Gómez-González J., Barcia A., 1990, A&A, 240, 116
Batrla W., Matthews H. E., Menten K. M., Walmsley C. M., 1987, Nat, 326, 49
Beuther H., Thorwirth S., Zhang Q., Hunter T. R., Megeath S. T., Walsh A. J., Menten K. M., 2005, ApJ, 627, 834
Beuther H., Walsh A. J., Thorwirth S., Zhang Q., Hunter T. R., Megeath S. T., Menten K. M., 2008, A&A, 481, 169
Breen S. L., Ellingsen S. P., Caswell J. L., Lewis B. E., 2010, MNRAS, 401, 2219
Brogan C. L., Hunter T. R., Cyganowski C. J., Indebetouw R., Beuther H., Menten K. M., Thorwirth S., 2009, ApJ, 707, 1
Brooks K. J., Garay G., Mardones D., Bronfman L., 2003, ApJ, 594, 131
Caswell J. L., 1997, MNRAS, 289, 203
Caswell J. L., 1998, MNRAS, 297, 215
Caswell J. L., 2009, Publ. Astron. Soc. Australia, 26, 454
Caswell J. L., Haynes R. F., 1987, Australian J. Phys., 40, 215
Caswell J. L., Vaile R. A., Ellingsen S. P., Whiteoak J. B., Norris R. P., 1995, MNRAS, 272, 96
Caswell J. L. et al., 2010, MNRAS, doi:10.1111/j.1365-2966.2010.16339.x
Chen X., Ellingsen S. P., Shen Z.-Q., 2009, MNRAS, 396, 1603
Codella C., Moscadelli L., 2000, A&A, 362, 723
Cragg D. M., Johns K. P., Godfrey P. D., Brown R. D., 1992, MNRAS, 259, 203
Cragg D. M., Sobolev A. M., Caswell J. L., Ellingsen S. P., Godfrey P. D., 2004, MNRAS, 351, 1327
Cyganowski C. J. et al., 2008, AJ, 136, 2391
Cyganowski C. J., Brogan C. L., Hunter T. R., Churchwell E., 2009, ApJ, 702, 1615
Davis C. J., Varricatt W. P., Todd S. P., Ramsay Howat S. K., 2004, A&A, 425, 981
De Buizer J. M., 2003, MNRAS, 341, 277
De Buizer J. M., Redman R. O., Longmore S. N., Caswell J., Feldman P. A., 2009, A&A, 493, 127
Ellingsen S. P., 2005, MNRAS, 359, 1498
Ellingsen S. P., 2006, ApJ, 638, 241
Ellingsen S. P., Cragg D. M., Lovell J. E. J., Sobolev A. M., Ramsdale P. D., Godfrey P. D., 2004, MNRAS, 354, 401
Ellingsen S. P., Voronkov M. A., Cragg D. M., Sobolev A. M., Breen S. L., Godfrey P. D., 2007, in Chapman J. M., Baan W. A., eds, Proc. IAU Symp. 242, Astrophysical Masers and their Environments. Cambridge Univ. Press, Cambridge, p. 213
Forster J. R., Caswell J. L., 1989, A&A, 213, 339
Furuya R. S., Cesaroni R., Takahashi S., Momose M., Testi L., Shinnaga H., Codella C., 2005, ApJ, 624, 827
Garay G., Reid M. J., Moran J. M., 1985, ApJ, 289, 681
Garay G., Moran J. M., Rodríguez L. F., Reid M. J., 1998, ApJ, 492, 635
Garay G., Brooks K. J., Mardones D., Norris R. P., 2003, ApJ, 587, 739

Gibb A. G., Davis C. J., 1998, MNRAS, 298, 644
Goedhart S., Gaylard M. J., van der Walt D. J., 2004, MNRAS, 355, 553
Goldsmith P. F., Mao X. J., 1983, ApJ, 265, 791
Goss W. M., Matthews H. E., Winnberg A., 1978, A&A, 65, 307
Green J. A. et al., 2009, MNRAS, 392, 783
Haschick A. D., Menten K. M., Baan W. A., 1990, ApJ, 354, 556
Henning Th., Lapinov A., Schreyer K., Stecklum B., Zinchenko I., 2000, A&A, 364, 613
Hill T., Burton M. G., Minier V., Thompson M. A., Walsh A. J., Hunt-Cunninham M., Garay G., 2005, MNRAS, 363, 405
Ho P. T. P., Klein R. I., Haschick A. D., 1986, ApJ, 305, 714
Keto E. R., Ho P. T. P., 1989, ApJ, 347, 349
Kirsanova M. S., Wiebe D. S., Sobolev A. M., 2009, Astron. Rep., 2009, 53, 611
Kogan L., Slysh V., 1998, ApJ, 497, 800
Kurtz S., Hofner P., Álvarez C. V., 2004, ApJS, 155, 149
Lees R. M., 1973, ApJ, 184, 763
Liechti S., Wilson T. L., 1996, A&A, 314, 615
Mehringer D. M., 1994, ApJS, 91, 713
Mehringer D. M., Menten K. M., 1996, ApJ, 474, 346
Menten K. M., 1991, ApJ, 380, L75
Menten K. M., Batrla W., 1989, ApJ, 341, 839
Menten K. M., Walmsley C. M., Henkel C., Wilson T. L., 1986, A&A, 157, 318
Müller H. S. P., Menten K. M., Mäder H., 2004, A&A, 428, 1019
Muños D. J., Mardones D., Garay G., Rebolledo D., Brooks K., Bontemps S., 2007, ApJ, 668, 906
Norris R. P., Whiteoak J. B., Caswell J. L., Wieringa M. H., Gough R. G., 1993, ApJ, 412, 222
Phillips C. J., Norris R. P., Ellingsen S. P., McCulloch P. M., 1998, MNRAS, 300, 1131
Plambeck R. L., Menten K. M., 1990, ApJ, 364, 555
Pratap P., Shute P. A., Keane T. C., Battersby C., Sterling S., 2008, AJ, 135, 1718
Rodríguez L. F., Garay G., Brooks K. J., Mardones D., 2005, ApJ, 626, 953
Salii S. V., Sobolev A. M., Kalinina N. D., 2002, Astron. Rep., 46, 955
Slysh V. I., Kalenskii S. V., Val'tts I. E., 1993, ApJ, 413, 133
Slysh V. I., Kalenskii S. V., Val'tts I. E., Otrupcek R., 1994, MNRAS, 268, 464
Slysh V. I., Val'tts I. E., Kalenskii S. V., Voronkov M. A., Palagi F., Tofani G., Catarzi M., 1999, A&AS, 134, 115
Sobolev A. M., 1992, SvA, 36, 590
Sobolev A. M., Deguchi S., 1994, A&A, 291, 569
Sobolev A. M., Strelnitskii V. S., 1983, Soviet Astron. Lett., 9, 12
Sobolev A. M., Ostrovskii A. B., Kirsanova M. S., Shelemei O. V., Voronkov M. A., Malyshev A. V., 2005, in Churchwell E., Conti P., Felli M., eds, Proc. IAU Symp. 227, Massive Star Birth: A Crossroads of Astrophysics. Cambridge Univ. Press, Cambridge, p. 174
Sutton E. C., Sobolev A. M., Ellingsen S. P., Cragg D. M., Mehringer D. M., Ostrovskii A. B., Godfrey P. D., 2001, ApJ, 554, 173
Sutton E. C., Sobolev A. M., Salii S. V., Malyshev A. V., Ostrovskii A. B., Zinchenko I. I., 2004, ApJ, 609, 231
Szymczak M., Pillai T., Menten K. M., 2005, A&A, 434, 613
Val'tts I. E., Ellingsen S. P., Slysh V. I., Kalenskii S. V., Otrupcek R., Larionov G. M., 2000, MNRAS, 317, 315
Voronkov M. A., 1999, Astron. Lett., 25, 149
Voronkov M. A., Sobolev A. M., Ellingsen S. P., Ostrovskii A. B., Alakoz A. V., 2005a, Ap&SS, 295, 217
Voronkov M. A., Sobolev A. M., Ellingsen S. P., Ostrovskii A. B., 2005b, MNRAS, 362, 995
Voronkov M. A., Brooks K. J., Sobolev A. M., Ellingsen S. P., Ostrovskii A. B., Caswell J. L., 2006, MNRAS, 373, 411
Voronkov M. A., Brooks K. J., Sobolev A. M., Ellingsen S. P., Ostrovskii A. B., Caswell J. L., 2007, in Chapman J. M., Baan W. A., eds, Proc. IAU Symp. 242, Astrophysical Masers and their Environments, Massive Star Birth: A Cross roads of Astrophysics. Cambridge Univ. Press, Cambridge, p. 182
Walsh A. J., Burton M. G., Hyland A. R., Robinson G., 1998, MNRAS, 301, 640
Walsh A. J., Macdonald G. H., Alvey N. D. S., Burton M. G., Lee J.-K., 2003, A&A, 410, 597
Walsh A. J., Chapman J. F., Burton M. G., Wardle M., Millar T. J., 2007, MNRAS, 380, 1703
Wilson T. L., Walmsley C. M., Menten K. M., Hermsen W., 1985, A&A, 147, L19
Wu Y., Qin S.-L., Guan X., Xue R., Ren Z., Liu T., Huang M., Chen S., 2009, ApJ, 697, L116

This paper has been typeset from a TEX/LATEX file prepared by the author.